Mon. Not. R. Astron. Soc. **318**, 535–546 (2000)

Starburst galaxies and structure in the submillimetre background towards the *Hubble Deep Field*

J. A. Peacock,[1★] M. Rowan-Robinson,[2] A. W. Blain,[3,4] J. S. Dunlop,[1] A. Efstathiou,[2] D. H. Hughes,[1,5] T. Jenness,[6] R. J. Ivison,[7] A. Lawrence,[1] M. S. Longair,[3] R. G. Mann,[1,2] S. J. Oliver[2,8] and S. Serjeant[2]

[1]*Institute for Astronomy, University of Edinburgh, Royal Observatory, Blackford Hill, Edinburgh EH9 3HJ*
[2]*Astrophysics Group, Imperial College, Blackett Laboratory, Prince Consort Road, London SW7 2BZ*
[3]*Cavendish Astrophysics Group, Cavendish Laboratory, Madingley Road, Cambridge CB3 0HE*
[4]*Institute of Astronomy, University of Cambridge, Madingley Road, Cambridge CB3 0HA*
[5]*Instituto Nacional de Astrofisica, Optica y Electronica (INAOE), Apartado Postal 51 y 216, 72000 Puebla, Pue., Mexico*
[6]*Joint Astronomy Centre, 660 N. A'ohoku Place, Hilo, Hawaii 96720, USA*
[7]*Department of Physics & Astronomy, University College London, Gower Street, London WC1E 6BT*
[8]*CPES, University of Sussex, Falmer, Brighton BN1 9QH*

Accepted 2000 June 8. Received 2000 June 8; in original form 1999 December 13

ABSTRACT

We use an 850-μm SCUBA map of the *Hubble Deep Field* (HDF) to study the dust properties of optically-selected starburst galaxies at high redshift. The optical/infrared (IR) data in the HDF allow a photometric redshift to be estimated for each galaxy, together with an estimate of the visible star-formation rate. The 850-μm flux density of each source provides the complementary information: the amount of hidden, dust-enshrouded star formation activity. Although the 850-μm map does not allow detection of the majority of individual sources, we show that the galaxies with the highest UV star-formation rates are detected statistically, with a flux density of about $S_{850} = 0.2$ mJy for an apparent UV star-formation rate of $1\,h^{-2}\,\mathrm{M}_{\odot}\,\mathrm{yr}^{-1}$. This level of submillimetre output indicates that the total star-forming activity is on average a factor of approximately 6 times larger than the rate inferred from the UV output of these galaxies. The general population of optical starbursts is then predicted to contribute at least 25 per cent of the 850-μm background. We carry out a power-spectrum analysis of the map, which yields some evidence for angular clustering of the background source population, but at a level lower than that seen in Lyman-break galaxies. Together with other lines of argument, particularly from the NICMOS HDF data, this suggests that the 850-μm background originates over an extremely wide range of redshifts – perhaps $1 \lesssim z \lesssim 6$.

Key words: galaxies: evolution – galaxies: starburst – cosmology: observations.

1 INTRODUCTION

The observational ingredients for an understanding of galaxy formation are arguably now largely in place. In particular, the Lyman-break technique has allowed the selection of galaxies over the redshift range $2 \lesssim z \lesssim 5$ (Steidel et al. 1996). The combination of ground-based and *Hubble Space Telescope* (*HST*) data has allowed such samples to probe a wide range of optical/UV luminosities, so that the statistical properties of the high-redshift galaxy population are increasingly well-known. This knowledge is conveniently summarized in the form of the global star-formation rate as a function of redshift. This function rises steeply between $z = 0$ and $z = 1$ (Lilly et al. 1996); initial indications from the HDF were that there was then a maximum, followed by a decline at $z \gtrsim 2$ (Madau et al. 1996). More recent Lyman-break data, however, have cast doubt on this claim: it now seems more likely that the UV luminosity density remains approximately constant for $2 \lesssim z \lesssim 5$ (Steidel et al. 1999). Nevertheless, since there is little cosmological time at $z > 5$, these results are often taken to suggest that we have seen almost all the star-formation that ever occurred. Provided we can understand the masses of the galaxies that are involved (as is starting to be possible though Balmer-line spectroscopy; Pettini et al. 1998), the entire history of the galaxy-formation process is potentially open to view.

The main objection to this optimistic picture is well known: star formation in the local universe is often accompanied by dust.

★ E-mail: jap@roe.ac.uk

There is thus the possibility that a large, or even dominant, component of the star-forming history is not revealed by optical/UV data. It has long been clear that this question would only be settled by studies in the far-infrared (FIR) or submillimetre bands, and great progress is now being made in this area. The total amount of energy released from young stars and reprocessed into emission from cool dust is constrained by the detection of the background radiation at $\lambda \gtrsim 150\,\mu$m (Puget et al. 1996; Schlegel, Finkbeiner & Davis 1998; Fixsen et al. 1998; Hauser et al. 1998). The resolution of this background into point sources has been made possible with the SCUBA imager on the James Clerk Maxwell Telescope (Holland et al. 1999). A number of groups have used this facility in order to map the submillimetre sky down to an rms sensitivity below 1 mJy at 850 μm (Smail, Ivison & Blaim 1997; Hughes et al. 1998; Blain et al. 1999; Barger, Cowie & Sanders 1999; Eales et al. 1999).

The observations of Hughes et al. (1998, hereafter H98) are the deepest of existing data sets, and also have the advantage that they cover the area of the northern *Hubble Deep Field* (*HDF*) (Williams et al. 1996). The galaxy population in this region of the sky has been studied in great detail, and so there is the potential to extract considerable information from the submillimetre data. The initial study by H98 considered only possible optical counterparts for the brightest five 850-μm sources. Here, the intention is to dig much more deeply into the background population. The optical HDF data tell us the location of a large number of starburst galaxies, and it should be possible to measure in a statistical way their submillimetre emission. In this way, we will learn about the fraction of the star-forming activity in these galaxies that is hidden from view. The existence of photometric redshifts means that we can do this as a function of redshift; this measurement is critical, because it will tell us whether or not to believe the indications from the optical/UV data that most of the star-formation in the universe has been seen.

In fact, there are already indications that a large fraction of the star-forming activity in the universe is not visible in the UV. From the first general detection of luminous infrared galaxies (e.g. Soifer et al. 1987), it has increasingly become clear that the majority of the star-forming activity at low redshift is extinguished by dust (e.g. Meurer et al. 1997). The same appears to be true at high redshift: for example, the brightest few sources in the HDF 850-μm map of H98 have very weak or no optical counterparts. If their submillimetre emission arises from star formation, all but of order 1 per cent of the activity is hidden. This is direct evidence that the 850-μm background contains a substantial contribution from ultraluminous infrared galaxies (ULIRGs), as has been found by a number of other authors (e.g. Barger et al. 1999; Lilly et al. 1999). Even where starburst galaxies are visible in the UV, measures of the star-formation rate (SFR) based on Balmer emission lines often gives rates up to 10 times larger than would be inferred from the UV continuum alone (Pettini et al. 1998). These latter corrections are often used to correct the observed UV luminosity density and thus estimate the total density of star-formation in the universe. The results of H98 show that this is dangerous, since there can also be an additional component of star-formation that is so heavily embedded that it fails to show up either in the UV or in the Balmer lines. The only way to detect such a component is through the submillimetre emission, which is the approach of this paper. The structure of the paper is as follows: Section 2 summarizes the optical HDF data and shows how to predict submillimetre emission from the HDF galaxies as a function of redshift, to within an unknown proportionality factor; Section 3 compares these predictions to the observed 850-μm data and shows that there is evidence that the 850-μm emission originates over the broad redshift range $1 \lesssim z \lesssim 6$; Section 4 attempts to test this picture by measuring the clustering of the submillimetre emission in the HDF map.

2 STARBURSTS IN THE HDF

2.1 Photometric redshifts

One great virtue of the HDF data is their wide wavelength coverage. This has allowed several groups to estimate redshifts and spectral types via a variety of template-fitting strategies. Generally, these work impressively well (see e.g. Hogg et al. 1998 and references therein). The catalogues of Fernandez-Soto, Lanzetta & Yahil (1999, hereafter FLY) have been particularly successful, as they incorporate *JHK* data. For the present work, we use a set of photometric redshifts constructed according to a similar philosophy at Imperial College (IC) (Rowan-Robinson, in preparation). A comparison of their results is shown in Fig. 1; generally, there is excellent agreement. The IC data base also provides redshift estimates for fainter galaxies, beyond the reach of near-IR data. Inevitably, these estimates will be less accurate, but are still worth including.

2.2 UV star-formation rates

Following Madau et al. (1996), we estimate the star-formation rate from the luminosity at a rest-frame wavelength of 1500 Å:

$$\frac{\mathrm{SFR}}{\mathrm{M}_\odot\,\mathrm{yr}^{-1}} = \frac{L_\nu(1500\,\text{Å})}{10^{21.0}\,\mathrm{W\,Hz}^{-1}}. \qquad (1)$$

A number of slightly different figures for this conversion can be found in the literature (e.g. Pettini et al. 1998; Steidel et al. 1999); the uncertainty in the appropriate conversion factor is however small compared to the uncertain degree of extinction. For redshifts $1 \lesssim z \lesssim 4.4$, this wavelength lies within the range of the WFPC2 data; for other redshifts, a small degree of extrapolation is required.

The spectral index can also be evaluated (using the two bands

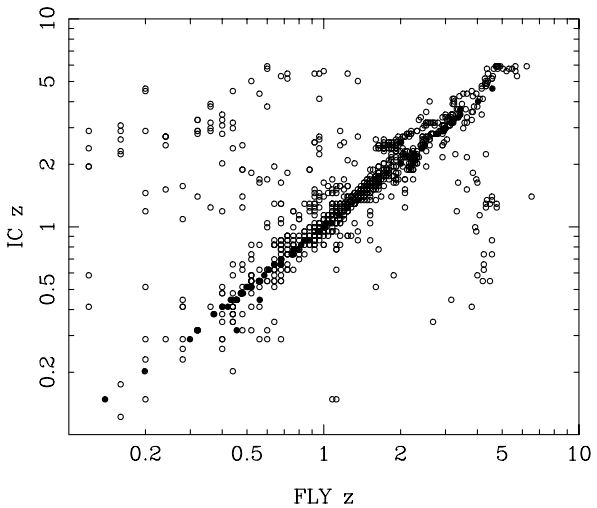

Figure 1. Comparison of photometric redshifts between the Imperial College group (Rowan-Robinson, in preparation) and Fernandez-Soto, Lanzetta & Yahil (1999) Solid points show spectroscopic redshifts (adopted for the x axis where known).

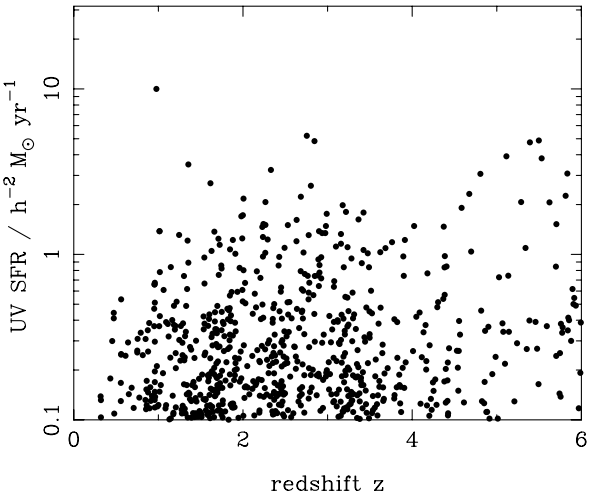

Figure 2. UV SFR against redshift. The raw SFR values are low in all cases, with only a handful of objects exceeding $5\,h^{-2}\,\mathrm{M}_\odot\,\mathrm{yr}^{-1}$.

closest to 1500 Å): $L_\nu \propto \nu^{-\alpha}$. Both the SFR and α require the data to be corrected for the effects of intergalactic absorption. We use the corrections given in fig. 1 of Madau et al. (1996), which may conveniently be approximated by

$$\frac{f_{\rm obs}}{f_{\rm emit}} = \exp[-(z/z_{\rm c})^{7.0}], \qquad (2)$$

with $z_{\rm c} = (2.50, 3.75, 4.65)$ for the $(U_{300}, B_{450}, V_{606})$ wavebands. For very high redshifts, these corrections become sufficiently large that they cannot be made reliably (given the uncertainty in redshift). Therefore, for $z > 4.5$, we assume a spectral index of zero and work from the observed magnitude at I_{814}.

Dust-free starbursts would normally be expected to have $\alpha \simeq 0$, whereas many of the HDF galaxies have redder spectra. Pettini et al. (1998) argue that this reddening is due to dust. They show that the star-formation rates for $z \simeq 3$ starbursts as inferred from Balmer lines are often much higher than those inferred from the UV flux, by up to a factor 10. Moreover, they claim that the reddest galaxies are those for which the correction factor is largest. The spectral indices could be used to produce corrected star-formation rates, but we shall not do this; the aim of this paper is to use the submillimetre emission to infer the total amount of hidden star formation, which can then be compared with the activity that is directly visible in the UV.

Fig. 2 shows the inferred star-formation rate for all HDF galaxies with photometric redshifts (assuming $\Omega = 1$ unless otherwise stated), plotted against redshift. The uncorrected rates are low, with only five galaxies exceeding $5\,h^{-2}\,\mathrm{M}_\odot\,\mathrm{yr}^{-1}$. We see that the most active galaxies are found rather uniformly over the redshift range $1.5 \lesssim z \lesssim 5$. To the extent that submillimetre flux density is a weak function of redshift at high z, this suggests that we would expect a similar redshift distribution for 850-μm sources.

2.3 Dust models and 850-μm emission

In order to make predictions of the 850-μm flux density, we use a simple single-temperature grey-body dust model, with $T = 50\,\mathrm{K}$ and an emissivity proportional to ν^β with $\beta = 1.5$. The luminosity at rest wavelength λ_0 is then

$$\frac{L_\nu}{\mathrm{W\,Hz^{-1}}} = 10^{23.0}\,h^{-2}\left(\frac{\mathrm{SFR}}{h^{-2}\,\mathrm{M}_\odot\,\mathrm{yr}^{-1}}\right)\frac{y^{-(3+\beta)}}{\exp(1/y)-1}, \qquad (3)$$

where $y = \lambda_0/288\,\mu\mathrm{m}$. The coefficient of proportionality was set by comparing with models for Arp220 (Hughes & Dunlop 1999); for a star-formation rate of $75\,h^{-2}\,\mathrm{M}_\odot\,\mathrm{yr}^{-1}$, we normalize to an 850-μm flux density of 2.5 mJy at $z = 3$. As is well known, such models predict a submillimetre flux density that is very nearly independent of redshift. For $z \gtrsim 1.5$, our assumptions give an SFR of approximately $30\,h^{-2}\,\mathrm{M}_\odot\,\mathrm{yr}^{-1}$ for a 1-mJy source.

Of course, the submillimetre luminosity is a not a measure of the total star-formation rate; rather, it measures the fraction that is heavily embedded. One way to deal with this would be to follow Pettini et al. (1998) and scale the UV SFR by a factor that depends on spectral index: SFR $\rightarrow f(\alpha)$SFR; the submillimetre emission would then be proportional to the corrected star-formation rate, times $[1 - 1/f(\alpha)]$. However, such a procedure implicitly assumes a simple geometry for the dust, and ignores the possibility of an extra contribution from heavily embedded star-formation regions. We shall therefore prefer to derive the relation between the visible and hidden SFRs empirically.

It is clear in advance that very substantial extinctions will be required if the HDF starburst galaxies are to be detectable in the submillimetre. The rms noise level of the 850-μm map is 0.45 mJy, so we require a flux density of 1 mJy for an individual detection, or several times 0.1 mJy in order to be able to achieve a statistical detection. The former figure corresponds to an SFR of about $30\,h^{-2}\,\mathrm{M}_\odot\,\mathrm{yr}^{-1}$, whereas we have seen that the uncorrected UV SFR figures generally lie more than a factor of 10 lower than this. In order to measure the hidden component, we shall use the term 'predicted' 850-μm flux density to denote the value that would be expected if the hidden SFR equalled the rate deduced from the UV continuum:

$$\frac{\text{hidden SFR}}{\text{visible SFR}} = \frac{\text{observed } S_{850}}{\text{predicted } S_{850}}. \qquad (4)$$

Of course, this makes the assumption that the submillimetre emission originates in starlight re-radiated by dust. All that is directly measured is the total amount of energy that is being re-radiated, independent of its origin.

3 STATISTICAL DETECTION OF OPTICAL STARBURSTS

3.1 Predicted SCUBA maps

One direct way in which we can try to see if the general starburst population contributes to the SCUBA data is to make synthetic maps. Rather than compare directly to the observed 850-μm map, we first construct a residual map, subtracting the five brightest sources (to a limit of 2 mJy) studied in H98. The rationale for this is that it is impossible to predict accurately the brightest few sources, which dominate the visual appearance of the map. On the other hand, the general background emission is affected by many objects, and we stand a better chance of seeing a correlation between predictions and observations. Fig. 3 shows the original and the residual map.

The residual map (Fig. 3b) shows considerable structure. There are a number of isolated regions of peak emission around 2 mJy, which are further candidates for point sources. Some of these clearly blend, such as the horizontal 'worm' structure just South of the map centre. This is an indication that the image is starting to approach the confusion limit. There is in addition a hint of a striped pattern, with large-scale areas of low and high emission. This pattern could be taken as a flat-fielding artefact, and a

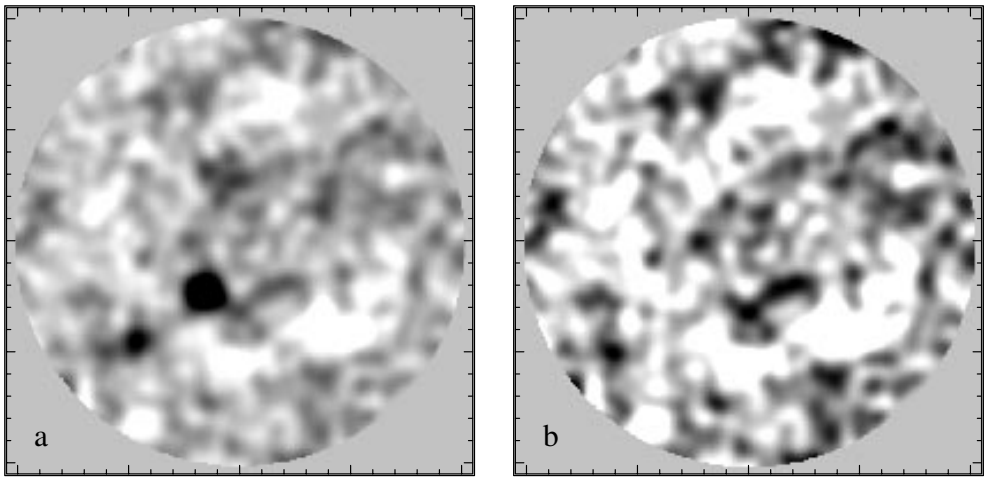

Figure 3. The 850-μm map of the HDF, with north to the top and east to the left. Panel (a) shows the raw map (in which five sources brighter than 2 mJy have been subtracted and restored with single Gaussian beams, in order to reduce the effects of sidelobes); panel (b) shows the residual map with these five sources removed. Both maps are 210-arcsec square; the frame has small tick marks at 10-arcsec intervals. Black denotes high flux; the map is set to zero beyond 100-arcsec radius. Both maps have been scaled to remove the trend for instrumental noise to increase with radius.

number of reduction strategies were tried, with the conclusion that it seemed to be a robust feature.

We now ask for the predicted appearance of the 850-μm sky, based on the UV starbursts. This is only possible over the subarea of the 850-μm map that overlaps the optical HDF, as shown in Figs 4a and b. The predicted 850-μm map is shown in Fig 4c; this represents a possible future view of the submillimetre sky, given an instrument with an effective aperture a few times larger than the JCMT. When convolved with the JCMT beam (including the effects of chopping and nodding), the simulated (noise-free) map of Fig. 4d is produced. As a match to the true sky, Fig. 4d has some successes and some failures. It does reproduce the character of the large-scale variations in emission. This encourages us to believe that features such as the prominent 'hole' to the bottom right (WF chip 4) do indeed result from a general lack of submillimetre sources in that region of the sky. Other features match less well, however: the predicted top central bright feature is absent in reality; there is no optical counterpart to the prominent horizontal blend just South of the map centre. This lack of a detailed match is entirely to be expected, given that there is a large contribution to the map from ULIRGs, which cannot be predicted from the HDF UV data.

3.2 Emission in redshift shells

It is interesting to dissect the predicted submillimetre emission as a function of redshift. It is entirely possible that the relative amounts of hidden and visible star formation could evolve as a function of redshift, causing one redshift band to dominate more than predicted. We therefore divided the map of Fig. 4d into the contributions from different redshift slices, and looked to see how well each correlated with the true map; the result is shown in Fig. 5. Although the correlation signals from different redshift shells are relatively noisy, there is a quite impressive trend with redshift, with little mean correlation at $z < 1$, but a positive signal broadly distributed over the higher-redshift bins – especially at $z > 2.5$. Figs 4e and f show the contributions to the predicted submillimetre map, divided at this redshift. This is direct evidence that, as expected from the SFR data in Fig. 2, the HDF map receives contributions from a very wide range of redshifts. The UV starburst galaxies thus contribute to the 850-μm background in a similar fashion to the ULIRG population, which has a median redshift of between 2.5 and 3 (H98; Smail et al. 2000).

Fig. 6 shows in detail the distribution of $z > 2.5$ galaxies (confined to the brighter objects, where the photometric redshifts should be more robust). This is clearly a very strongly clustered distribution, as found by Steidel et al. (1998). Perhaps the most striking feature is the lack of galaxies in the region where the SCUBA map shows its deepest 'hole'. Although we do not necessarily expect a very precise match between the observed and the predicted S_{850} for a given object, the existence of large-scale features in a clustered galaxy distribution will induce structure in the 850-μm map. We will return to this point in Section 4 below, where we quantify the degree of clustering in the submillimetre background.

3.3 The amount of hidden star formation

Perhaps the most direct way of seeing if we are detecting the effect of the UV starbursts on the 850-μm map is to estimate a flux density for each galaxy, and look for a correlation between predicted and observed flux densities. We therefore take the value of the residual map at the position of each UV source as the best estimate of its true 850-μm flux density.

These observed flux densities are plotted against redshift in Fig. 7. This is a scatter diagram, with no correlation. However, a very different picture emerges when we plot 850-μm flux density against UV SFR, as in Fig. 8. Much of this plot is also a scatter diagram, but closer inspection reveals a clear tendency for the objects of highest star-formation rate to have positive fluxes. There is a group of sources with $S_{850} \gtrsim 1$ mJy and SFR $\gtrsim 2h^{-2}\,\mathrm{M}_{\odot}\,\mathrm{yr}^{-1}$ that stand out as plausible real detections. The parameters for these sources are listed in Table 1. Averaging the data in bins yields mean values for the flux density at a given SFR, and these results are also shown in Fig. 8. This demonstrates that we are able to achieve a clear statistical detection of 850-μm emission from optically selected galaxies even at a level down to 0.1 mJy.

It is interesting to contrast this result with the direct approach of pointed observations of individual Lyman-break galaxies, which

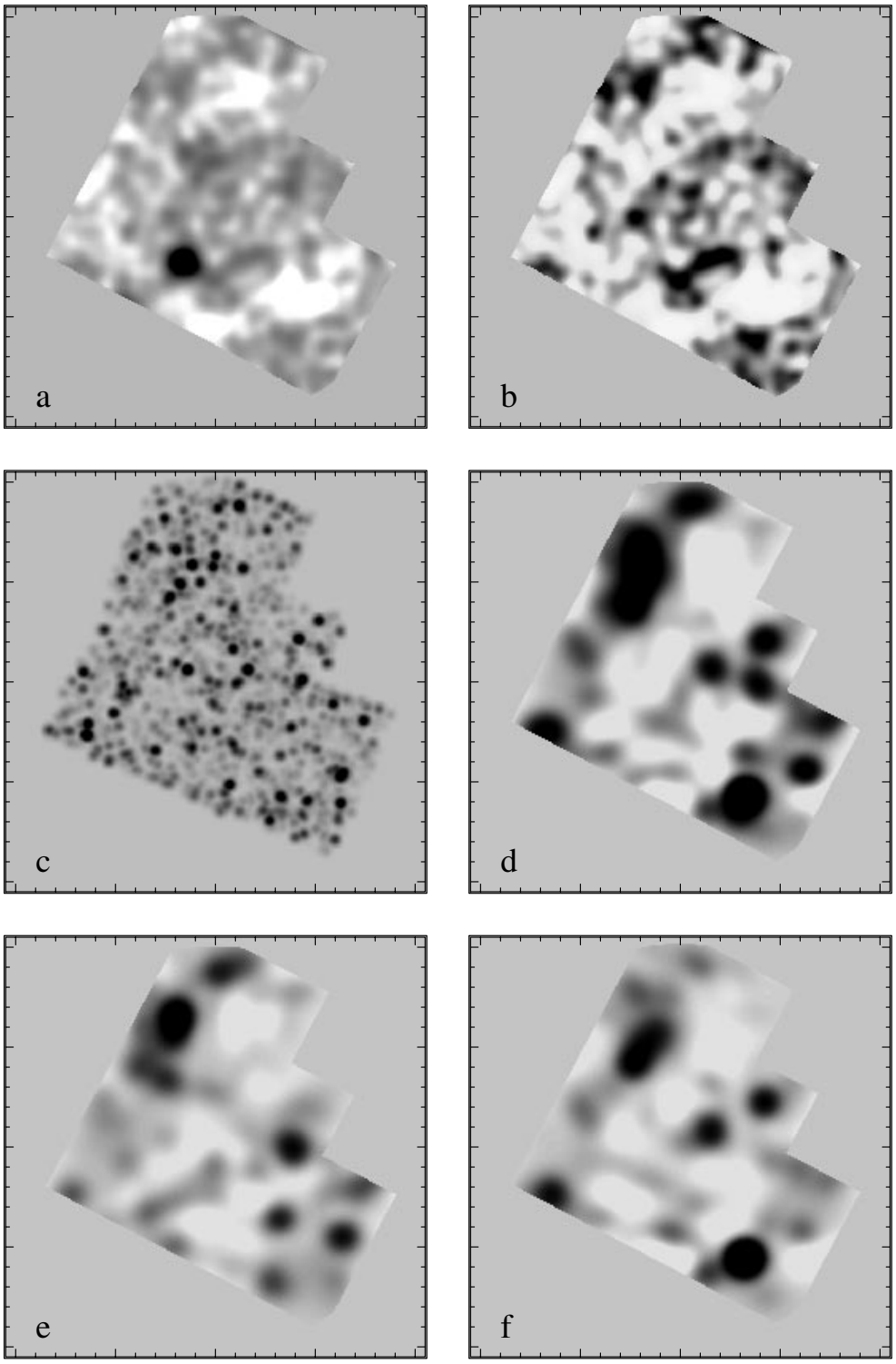

Figure 4. (a) The observed SCUBA 850-μm map, with north to the top and east to the left, windowed over the area of the HDF. The frame plotted is 200-arcsec square; (b) The SCUBA residual map, with the five brightest sources (>2 mJy) subtracted; (c) The predicted 850-μm map at high resolution; (d) The predicted 850-μm map with the SCUBA beam: (e) and (f) The same as (d) for respectively, $z < 2.5$ and $z > 2.5$. Different grey-scales are used in each case, to bring out the detail of interest in a given map. The frames show small tick marks at 10-arcsec intervals.

generally yield upper limits of a few mJy (e.g. Chapman et al. 1999). The statistical approach clearly needs a little thought, since we cannot be certain of the detection of any individual source. For example, many of the features on the HDF map are probably blends of a number of sources, so is there not a danger that we might be overestimating the mean flux from any individual source by also counting its neighbours? In fact, there is no such bias, at least for a Poisson-distributed field of sources (we consider the effect of clustering in Section 4 below). For a Poisson distribution, the expectation value of the flux contributed by all neighbours is

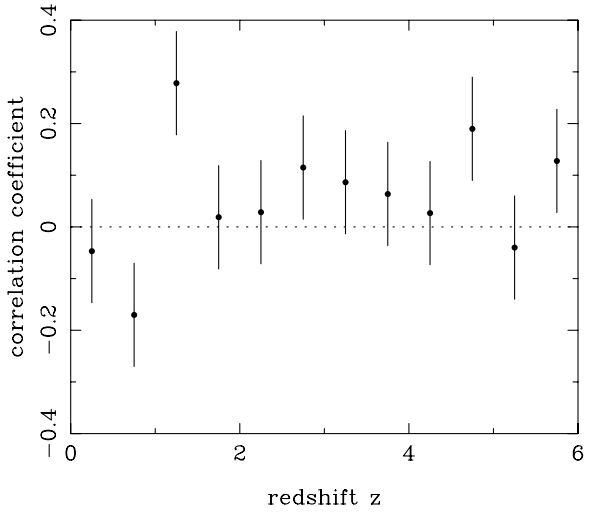

Figure 5. The cross-correlation coefficient between the 850-μm residual map and the projected UV emission from different redshift shells. The error bars were estimated by rotating the SCUBA map relative to the optical HDF data. Although no single redshift shell shows a strongly significant cross-correlation signal, there is a significant general level of correlation between the SCUBA data and the high-redshift galaxy distribution, broadly distributed over the redshift range $z > 1$.

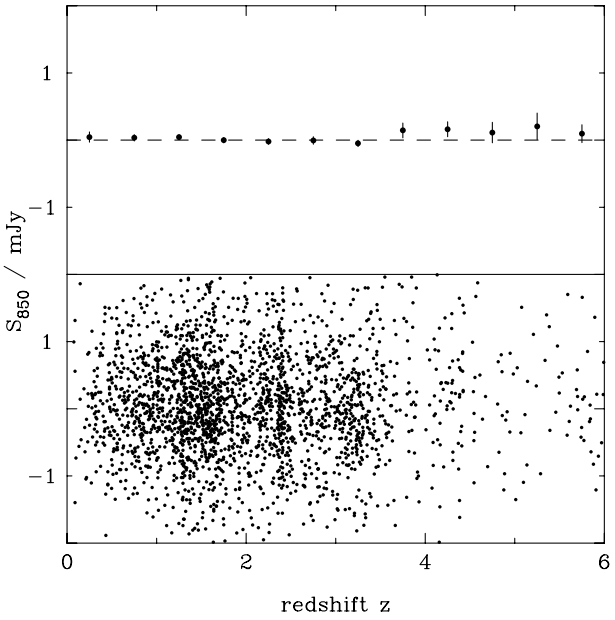

Figure 7. Observed 850-μm flux density against redshift. The bottom panel shows the raw values; the top shows mean values with standard errors.

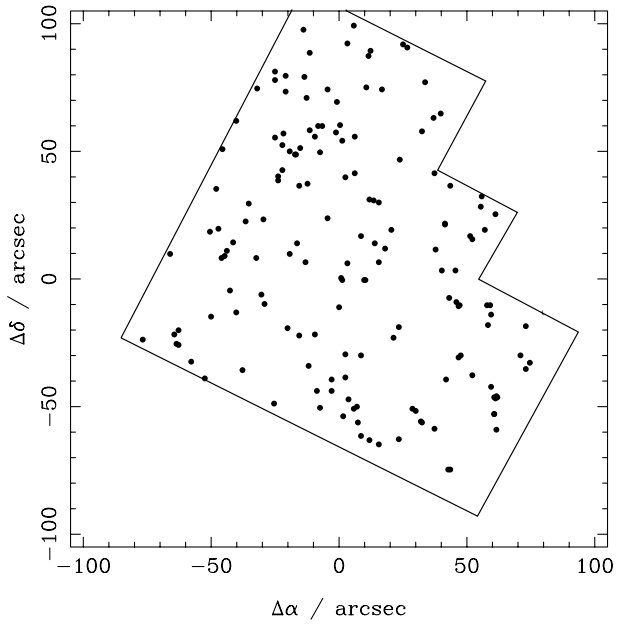

Figure 6. The brighter ($I_{814} < 27$) starburst galaxies at $z > 2.5$. There is a striking 'hole' in the distribution, centred on $(x, y) = (40, -40)$, corresponding to the observed lack of emission in the SCUBA map.

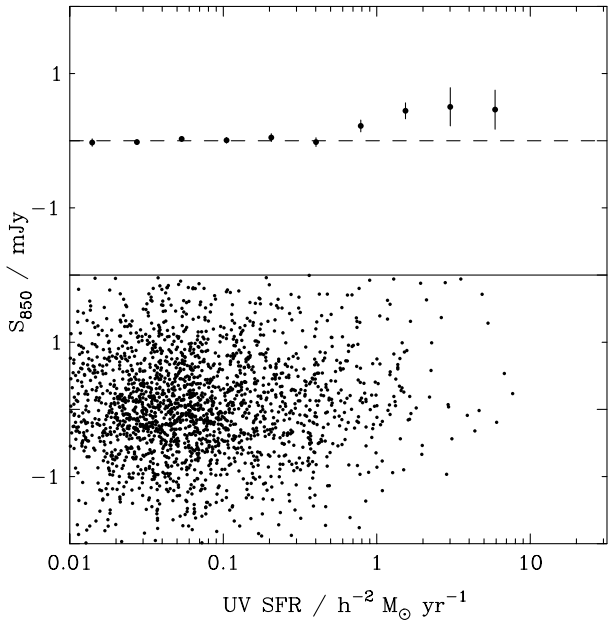

Figure 8. Observed 850-μm flux density against UV SFR. The bottom panel shows the raw values; the top shows mean values with standard errors.

just the mean flux on the map, which is zero owing to the chop-nod observing mode. Clearly, the effect of blends contributes a confusion-noise term to the general rms on the map, and this makes it harder to detect any given source. However, the instrumental noise dominates the rms in practice, so this is a minor effect. Even though there are a finite number of samples of noise on the map, each randomly-placed source gives a statistically independent sampling of this noise distribution, so the normal statistics of mean and standard error can be applied.

The mean and standard error of the submillimetre flux density to SFR ratio inferred from the points in Fig. 8 is

$$S_{850}/\mathrm{mJy} = 0.20 \pm 0.04 \frac{\mathrm{SFR}}{h^{-2}\,\mathrm{M}_\odot\,\mathrm{yr}^{-1}}. \quad (5)$$

This implies that the hidden star formation significantly exceeds that visible in the UV. A direct fit to the ratios of observed and predicted flux densities gives

$$\frac{\text{hidden SFR}}{\text{visible SFR}} = 4.25 \pm 1.2. \quad (6)$$

Table 1. The submillimetre properties of HDF sources with the largest star-formation rates ($>2h^{-2}\,M_\odot\,yr^{-1}$). True photometric redshifts are denoted by an asterisk.

Name	I_{814}	V_{606}	B_{450}	U_{300}	α	z_{IC}	z_{FLY}	SFR	S_{850}^{pred}/mJy	S_{850}^{obs}/mJy
2-449.0	23.39	23.68	23.92	25.72	0.32	2.85*	…	4.84	0.16	1.71
2-449.1	23.47	23.72	23.95	25.62	0.65	2.01*	2.01*	2.17	0.06	1.63
2-454.0	24.19	24.40	24.58	26.16	0.25	2.68	2.04	2.23	0.07	0.99
2-736.0	21.98	22.26	22.37	22.98	1.31	1.36*	…	3.50	0.09	1.94
2-736.11	22.94	23.11	23.16	23.71	1.07	1.62	…	2.69	0.07	1.89
3-82.0	25.25	26.68	28.25	…	…	5.84	0.60	3.08	0.14	−0.19
3-289.0	24.66	26.43	28.01	…	…	5.50	0.92	4.88	0.22	0.23
3-378.0	25.63	27.37	…	…	…	5.62	1.00	2.06	0.09	0.04
3-571.0	24.79	25.92	27.26	…	…	5.11	0.72	3.91	0.17	−0.09
3-839.0	24.66	26.82	28.92	…	…	5.39	2.08	4.75	0.21	−0.32
3-951.0	25.58	28.06	…	…	…	5.81	…	2.26	0.11	0.85
3-965.1112	25.53	26.89	29.33	…	…	5.29	…	2.07	0.09	−0.97
4-439.1	24.96	26.03	…	…	…	4.81	4.32	3.07	0.13	0.07
4-445.0	23.71	24.08	24.28	25.79	0.50	2.27*	2.27*	2.07	0.06	−0.54
4-454.0	20.99	20.79	20.68	20.97	0.65	0.98	…	10.00	0.26	−2.37
4-555.1	23.17	23.41	24.10	…	1.79	2.75	…	5.21	0.17	1.28
4-555.12	23.94	24.21	24.98	…	2.00	2.80*	2.88	2.60	0.09	1.37
4-639.2	25.22	26.18	28.44	…	…	4.67	4.16	2.32	0.10	0.18
4-776.0	24.94	26.64	…	…	…	5.53	0.96	3.80	0.17	0.53
4-878.11	23.22	23.53	23.93	25.48	1.10	2.33	0.00	3.24	0.10	−0.44

It is possible that this figure may be an underestimate. Examining the entries in Table 1 in more detail, it is apparent that there are a number of objects with estimated $z > 5$ for which: (a) the IC and FLY estimates disagree; (b) the observed flux densities scatter around zero. The estimated redshifts can tend to be unreliable at the extremes, owing to detection in only a few bands, so it is possible that the sample is corrupted by objects whose apparent high SFR is due to an erroneously large estimated z. If the above exercise is repeated, excluding objects with $z_{est} > 5$, the figures increase by about 1σ:

$$S_{850}/\mathrm{mJy} = 0.25 \pm 0.03 \frac{\mathrm{SFR}}{h^{-2}\,M_\odot\,yr^{-1}}; \quad (7)$$

$$\frac{\text{hidden SFR}}{\text{visible SFR}} = 6.85 \pm 1.53. \quad (8)$$

An alternative approach is to repeat the entire exercise using only the FLY redshift estimates; again the effect is to raise the level of the statistically detected S_{850} by very nearly 1σ.

It is worth asking if these results are consistent with the findings of Chapman et al. (1999), who carried out SCUBA photometry of eight Lyman-break galaxies, obtaining only one clear detection. The data in their Table 1 gives the ratio between 850-μm flux density and SFR, which has a typical rms error of 0.2 for an individual object. If fact, the scatter of their values is about twice this figure, apparently indicating a real scatter in properties. It is therefore appropriate to evaluate an unweighted mean and standard error, which gives

$$S_{850}/\mathrm{mJy} = 0.13 \pm 0.14 \frac{\mathrm{SFR}}{h^{-2}\,M_\odot\,yr^{-1}}; \quad (9)$$

this is a lower figure than our detection, but is statistically perfectly consistent with it.

Taking the various estimates discussed above, we adopt a best guess for the hidden-to-total ratio of

$$\frac{\text{hidden SFR}}{\text{visible SFR}} = 5 \pm 1.5. \quad (10)$$

This is unfortunately a rather model-dependent number, since it is sensitive to the spectral shape assumed in the submillimetre: the predicted 850-μm flux density scales roughly as $T^{-3.5}$ for a fixed bolometric luminosity, so moderate changes to the temperature can significantly alter the SFR inferred from a given 850-μm measurement. Nevertheless, this correction factor for the total SFR is similar to the mean correction inferred by Pettini et al. (1998), and other pieces of evidence are consistent with their results. Where reliable spectral indices can be deduced for the sources in Table 1, they are large and positive, ranging between 0.3 and 2.0. This is in agreement with the claim by Pettini et al. that a red UV continuum correlated with a high mean level of extinction. Similar arguments were also advanced by Meurer, Heckman & Calzetti (1999); they used the observed UV spectra of HDF galaxies to predict submillimetre fluxes, and their predicted results are in broad agreement with our data.

However, one should not assume a physical picture in which a foreground dust screen extinguishes a dust-free starburst. In a sense, all star formation is dust-enshrouded in that stars are born in dusty molecular clouds. Jimenez et al. (2000) argue that it takes about 15 Myr for young massive stars to burn away this dust and become visible. For continuous star formation, the hidden-to-visible SFR ratio is then really just a ratio of the time spent enshrouded, to the remaining lifetime of the stars once they are visible. Jimenez et al. (2000) argue that this ratio should be about 6:1 for a Salpeter IMF, and this is not inconsistent with our results. It is only possible to exceed this ratio if all star-forming regions are seen at an early phase, corresponding to a single dominant starburst; in this case, the optical counterpart will take the form of an ERO (e.g. Smail et al. 1999), or will be completely undetectable.

3.4 Contribution of Lyman-break galaxies to the background

If the true volume density of star formation is about 6 times what is visible is the UV, we need to be sure that this is consistent with the counts and background at 850 μm. The background is related to the proper volume emissivity, j_ν, as a function of redshift by

$$I_\nu(\nu_0) = \frac{1}{4\pi}\frac{c}{H_0}\int j_\nu[(1+z)\nu_0]\frac{\mathrm{d}z}{(1+z)^{11/2}} \quad (11)$$

(for $\Omega = 1$; see e.g. chapter 3 of Peacock 1999).

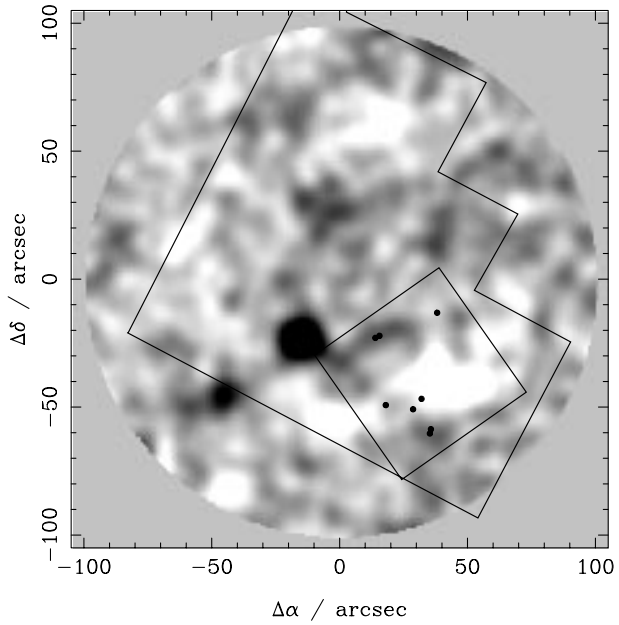

Figure 9. The NICMOS candidate ultrahigh-redshift galaxies are shown as points. Interestingly, these appear to coincide with weak SCUBA sources in the case of the two close pairs.

Table 2. The submillimetre properties of HDF/NICMOS candidate high-redshift galaxies.

Name	H_{160}	J_{110}	$S_{850}^{\rm obs}$/mJy
96.0	28.81	28.51	−0.15
118.0	27.86	28.65	1.88
123.0	28.08	…	1.95
150.0	26.39	27.21	−1.16
184.0	26.80	26.48	−0.19
248.0	28.13	28.10	0.10
266.0	28.76	…	1.27
678.0	27.93	27.60	1.35

Given the comoving redshift-dependent SFR density, it is easy to use this expression to evaluate the background. We use the UV density estimated by Steidel et al. (1999), with an assumed hidden-to-visible ratio of 5. Integrating to $z = 5$ gives a predicted background of

$$\nu I_\nu^{850}({\rm Lyman-break}) = 5.5 \times 10^{-10}\,{\rm W\,m^{-2}\,sr^{-1}}, \quad (12)$$

which is approximately identical to the total background ($5 \pm 2 \times 10^{-10}\,{\rm W\,m^{-2}\,sr^{-1}}$) estimated by Fixsen et al. (1998). This figure could be increased still further, by a factor of about 1.5, if we had adopted the corrections suggested by Steidel et al. to allow integration over the whole UV luminosity function. Alternatively, the estimate might be too high by a similar factor, because the SFR density at $z \lesssim 2$ is deduced from luminosities at 2800 Å, and these give systematically larger SFR figures for the more luminous starbursts in this paper. Both these corrections are within the statistical uncertainty on the SFR density.

Normal star-forming galaxies thus clearly make a very significant contribution to the submillimetre background, perhaps the dominant one. At the bright flux densities investigated by H98, all sources had hidden-to-visible SFR ratios that exceeded 60, so ULIRGs dominate the background in this flux regime, which contributes roughly 30 per cent of the Fixsen et al. background. Active galaxies may contribute up to a further 10 per cent (Almaini, Lawrence & Boyle 1999; Gunn & Shanks 1999). Taking the formal uncertainties on the background and on the hidden-to-total ratio, the 95 per cent lower confidence limit on the contribution of UV starburst galaxies to the background is 48 per cent, which is just consistent with the other contributions. This figure could be lowered in one of two ways: (i) if the true background were higher than estimated by Fixsen et al. (1998); (ii) if this analysis has overestimated the 850-μm flux density that corresponds to a given UV SFR. As discussed in Section 4, the only way in which the second effect might occur is as a result of clustering in the background population. In this case, the effective submillimetre emission might be overestimated by up to a factor 2. Even in this extreme case, however, the UV starbursts must generate a minimum of 25 per cent of the 850-μm background. We note that this empirical conclusion is in agreement with detailed attempts to fit the faint optical galaxy counts with models that include a dust correction to the SED, thus predicting also the contribution of normal galaxies to the submillimetre background (Busswell & Shanks 2000).

3.5 Comparison with NICMOS data

To obtain accurate estimated redshifts at $z \gtrsim 4$, infrared data are required. Part of the HDF (mainly chip WF4) has been imaged in *JHK* by Thompson et al. (1999). On the basis of the optical–infrared colours, 8 candidates for galaxies at extreme redshifts were identified (Weymann et al., in preparation), including the $z = 5.60$ object HDF4-473.0 (NICMOS source 184.0) studied by Weymann et al. (1998). The distribution of these objects is shown in Fig. 9, and their parameters are listed in Table 2. Although no significant submillimetre emission is associated with HDF4-473.0, there is a striking association between the two very close pairs of NICMOS objects and the two main 850-μm peaks in the NICMOS field – even extending to an agreement in position angle between the northernmost pair and the linear submillimetre source mentioned earlier. Given the lack of a plausible candidate identification for this object within the optical HDF catalogue, the case for association with a $z \gtrsim 5$ galaxy seems rather compelling.

4 BACKGROUND CLUSTERING ANALYSIS

4.1 Angular power spectrum

In order to improve on the somewhat anecdotal indications of clustering in the 850-μm map, possibly associated with high-redshift galaxies, it is necessary to quantify the degree of anisotropy seen in the map. The most direct tool for this is power-spectrum analysis, which allows a simple decomposition of the various contributions to the map. The map intensity, I, can be written as

$$I = (S^* W_1 + N) \times W_2, \quad (13)$$

where S is the true sky surface brightness; W_1 is the 'window function' corresponding to the instrumental beam (including negative sidelobes from chopping and nodding); N is the noise, which varies with radius; W_2 is a 'censor' function that sets the map to zero beyond 100-arcsec radius, and is also chosen with a radial variation to make the apparent noise independent of radius.

The structure in the sky background emission can be described either by its angular correlation function, $w(\theta)$, or by the angular

power spectrum, which is best written in dimensionless form as Δ^2_ℓ, the fractional variance per logarithmic increment of wavenumber:

$$w(\theta) = \int_0^\infty \Delta^2_\ell J_0(\ell\theta)\,\mathrm{d}\ell/\ell \qquad \Delta^2_\ell = \ell^2 \int_0^\infty w(\theta) J_0(\ell\theta)\theta\,\mathrm{d}\theta. \tag{14}$$

The angular wavenumber is written as multipole number, ℓ, to emphasize that the sky should really be expanded in spherical harmonics, $Y_{\ell m}$. However, our survey subtends a small enough angle that Fourier methods are an excellent approximation. For power-law clustering, $w(\theta) = (\theta/\theta_0)^{-\epsilon}$, this gives

$$\Delta^2_\theta(\ell) = (\ell\theta_0)^\epsilon 2^{1-\epsilon} \frac{\Gamma(1-\epsilon/2)}{\Gamma(\epsilon/2)}, \tag{15}$$

which is equal to $0.77(\ell\theta_0)^\epsilon$ for $\epsilon = 0.8$. This is the canonical slope for the small-separation correlations of local galaxies, which seems to evolve remarkably little with redshift (Giavalisco et al. 1998).

4.2 Window functions

An interesting aspect of the 850-μm HDF data set is that it contains a number of distinct scales, all of similar magnitude. The small-scale instrumental noise has an effective FWHM of 8.5 arcsec; the telescope beam has a FWHM of 14.7 arcsec, and chop throws of 30 and 45 arcsec; finally, the map radius is 100 arcsec, although the noise doubles at radius 90 arcsec. Each of these numbers controls the apparent clustering signal through an appropriate window function.

The window for the beam is most easily evaluated as a two-step process. Convolve the sky with a 14.7-arcsec FWHM Gaussian, then write the signal as $S = S_3 - (S_1 + S_2 + S_4 + S_5)/4$, where (1, 2, 3, 4, 5) label the positions in the chop/nod sequence. The variance for this sum is easily written down in terms of the correlation function of the smooth sky, which allows the window function to be identified:

$$|\tilde{W}_1|^2 = \tfrac{5}{4} + \tfrac{1}{4}J_0(\ell\theta) - J_0(2\ell\theta) - J_0(3\ell\theta) + \tfrac{1}{8}J_0(4\ell\theta) + \tfrac{1}{4}J_0(5\ell\theta) + \tfrac{1}{8}J_0(6\ell\theta), \tag{16}$$

where $\theta = 15$ arcsec.

The noise in the published (slightly smoothed) map has an rms of 0.45 mJy in the map centre, with a coherence length corresponding to filtering with a Gaussian of FWHM 8.5 arcsec. The spatial variation in the noise rms is divided out, so that the censoring function is

$$W_2 = [1 + (r/90\,\mathrm{arcsec})^2]^{-1}; \qquad r < R \equiv 100\,\mathrm{arcsec}. \tag{17}$$

Without the radial variation, the ℓ-space window would be just $\tilde{W}_2 = \tilde{W}_3$, where

$$\tilde{W}_3 = 2J_1(\ell R)/(\ell R); \tag{18}$$

a good approximation to the effect of the radial variation is to model $\tilde{W}_2$ by the expression for $\tilde{W}_3$, but decreasing the effective value of R to 85 arcsec.

4.3 Shot noise versus true clustering

The power spectrum of the observed map is a sum of three terms: instrumental noise, clustering of the background galaxies, and shot noise arising because the number of background galaxies is finite.

If all sources in the map had the same flux density, the shot noise would be just

$$\Delta^2_{\mathrm{shot}} = \frac{\ell^2}{2\pi N}, \tag{19}$$

where N is the surface density of sources. In the practical case where the sources have different flux densities, with number count $\mathrm{d}N(S)$, the effective value of N is

$$N_{\mathrm{eff}} = \frac{[\int S\,\mathrm{d}N(S)]^2}{\int S^2\,\mathrm{d}N(S)}. \tag{20}$$

For Euclidean counts, $\mathrm{d}N \propto S^{-5/2}\,\mathrm{d}S$, and the shot noise diverges at high flux densities. It therefore makes sense to work with the residual map where the brighter point sources have been subtracted. This is possible to a limit of 2 mJy in the 850-μm HDF map.

Blain et al. (1999) have shown that the number counts to 0.5 mJy are very close to Euclidean in form, with a normalization of

$$N(>1\,\mathrm{mJy}) = 7900 \pm 3000\,\mathrm{deg}^{-2}. \tag{21}$$

If we assume that Euclidean counts with $\mathrm{d}N = AS^{-5/2}\,\mathrm{d}S$ hold between 2 mJy and some flux density S_0, then

$$N_{\mathrm{eff}} = \frac{\sqrt{2}A}{S_0}(1 - \sqrt{S_0/2}) \tag{22}$$

The background intensity is

$$I = \int_{S_0}^\infty S\,\mathrm{d}N(S) = 2AS_0^{-0.5} \tag{23}$$

The observed background at 850 μm is

$$\nu I = 5 \pm 2 \times 10^{-10}\,\mathrm{W\,m^{-2}\,sr^{-1}} = 0.0033\,\mathrm{mJy\,arcsec^{-2}} \tag{24}$$

(Fixsen et al. 1998), so the observed count normalization ($A = 11850$) requires $S_0 = 0.31$ mJy, implying $N_{\mathrm{eff}} = 32800\,\mathrm{deg}^{-2}$.

It is unrealistic to assume abruptly truncated counts, and indeed Blain et al. (1999) present evidence that the counts have flattened by 0.5 mJy. Consider therefore the model

$$\frac{\mathrm{d}N}{\mathrm{d}S} = \frac{AS^{-5/2}}{1 + (S/S_0)^{-\gamma}}, \tag{25}$$

which is a more general variant of the form proposed by Barger, Cowie & Sanders (1999). We have no direct constraints on γ, but comparison with the faint cm-wavelength counts suggests $\gamma = 1$, and we adopt this value. The background is then $I = \pi A S_0^{-1/2}$, and the surface density above 1 mJy is $2AS_0^{-3/2}[S_0^{1/2} - \arctan(S_0^{1/2})]$. The observed counts and background then require $A = 16500$, $S_0 = 0.7$ mJy, and the effective shot-noise source density is $N_{\mathrm{eff}} = 92600\,\mathrm{deg}^{-2}$. This is probably a more realistic estimate than the previous figure; nevertheless, we have altered N_{eff} by a factor of three through different models for the faint counts, so this number has to be considered somewhat uncertain. Fortunately, it can be estimated directly from the data, as shown below.

4.4 Results

Fig. 10 shows the observed power spectrum estimated from the 850-μm map. The analysis requires a dimensionless fluctuation field, so the map (after bright-source subtraction) was divided by the expected background from sources at $S < 2$ mJy, which is 0.66

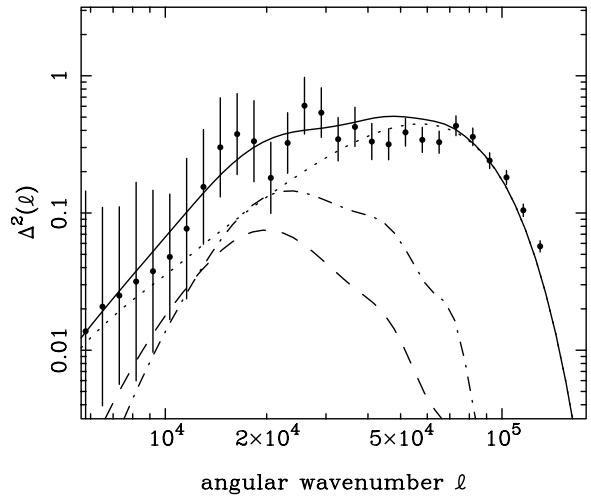

Figure 10. The 2D power spectrum of the 850-μm HDF map. Angular wavenumber is denoted by ℓ, and $\Delta^2(\ell)$ is the contribution to the fractional sky variance from unit range of $\ln \ell$. The dotted line shows the expected noise spectrum; the dot-dashed line is the shot noise component for an effective surface density of $N_{\rm eff} = 92600\,{\rm deg}^{-2}$ (see text); the dashed line is the contribution from clustering with $\theta_0 = 1$ arcsec; the solid line is the total model power, which fits the data well.

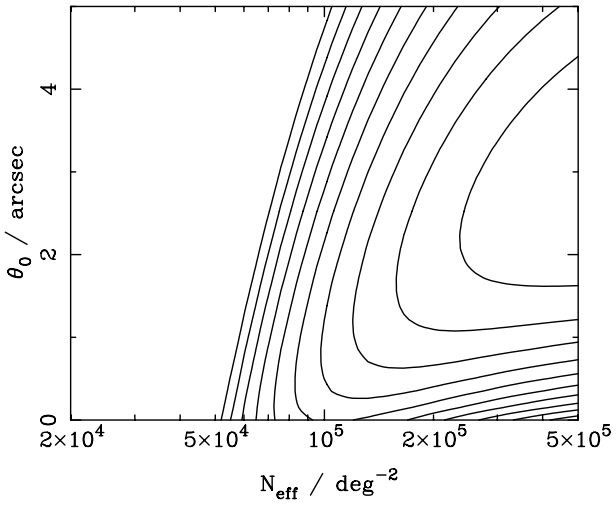

Figure 11. Contours of likelihood relative to maximum for the fit of the 850-μm power spectrum data by a combination of shot noise (effective surface density for sources with flux density <2 mJy $N_{\rm eff}$) and galaxy clustering (where θ_0 is the scale-length in the angular correlation function). The contour interval is 0.5 in $\ln \mathcal{L}$, corresponding to confidence contours of approximately 39, 63, 78, 87, 92 per cent etc.

of the total, according to the above count model, equivalent to a flux density of 0.54 mJy per 14.7-arcsec beam. The power spectrum was deduced according to the methods described in Feldman, Kaiser & Peacock (1994). These authors showed that power estimates are correlated over wavenumber separations of order the reciprocal of the survey size, and this effect is noticeable for $\ell \lesssim 2\times10^4$.

The data are compared with a model which is a sum of instrumental noise, clustering, and shot noise. These intrinsic effects are modified in two ways by instrumental effects: the small-scale power is reduced by filtering with the telescope beam (introducing a factor $|\tilde{W}_1|$), and the large-scale power is reduced because the map is constrained to have zero mean flux (Peacock & Nicholson 1991); we cannot detect structures larger than the map size, so the observed power must go to zero at zero wavenumber (introducing a factor $[1-|\tilde{W}|^2]$). The overall model is thus

$$\Delta^2_{\rm obs} = (\Delta^2_{\rm clus} + \Delta^2_{\rm shot}) \times |\tilde{W}_1|^2 \times (1-|\tilde{W}_2|^2) + \Delta^2_{\rm noise} \times (1-|\tilde{W}_3|^2) \quad (26)$$

Shot noise is distinguishable from true clustering because these effects have a different dependence on scale. Our data cover only a restricted range of scales, so in practice we shall assume that the true angular clustering has a correlation structure of the same shape as is observed for most faint galaxy samples, but with an unknown amplitude: $w(\theta) = (\theta/\theta_0)^{-0.8}$.

Fig. 10 shows an illustrative fit of shot noise with $N_{\rm eff} = 92600\,{\rm deg}^{-2}$ as estimated above, and clustering with $\theta_0 = 1$ arcsec. However, both these parameters can be fitted to the data in the usual maximum likelihood manner. The result of this exercise is shown in Fig. 11. As would be expected, there is a degree of degeneracy in the free parameters; the data indicate an excess of power in the residual map above pure noise for $10^4 \lesssim \ell \lesssim 5\times10^4$, and this constrains the sum of clustering and shot power. The different scale dependencies of the two signals mean that the degeneracy is broken, and the preferred model has significant clustering ($\theta_0 = 3$ arcsec) and low shot noise ($N_{\rm eff} = 5\times10^5\,{\rm deg}^{-2}$). However, this is an unrealistically high surface density; we should really fix $N_{\rm eff}$ at its a priori estimated value, in which case there is no significant detection of clustering, and $\theta_0 = 3$ arcsec can be ruled out at approximately 95 per cent confidence.

4.5 Implications for origin of the background

What is the interpretation of the relatively weak angular clustering? The angular power is a projection of the true 3D spatial power spectrum, given by the k-space version of Limber's equation:

$$\Delta^2_\theta = \frac{\pi}{\ell} \int \Delta^2(\ell/y) C(y) y^5 \phi^2(y)\,{\rm d}y \quad (27)$$

(Kaiser 1992; see section 16.6 of Peacock 1999). In this expression, y is the comoving angular-diameter distance, and the 'selection function' $\phi(y)$ is normalized so that

$$\int_0^\infty y^2 \phi(y) C(y)\,{\rm d}y = 1. \quad (28)$$

The curvature factor

$$C(y) = \left[1 + \frac{(1-\Omega)y}{c/H_0}\right]^{-1/2}, \quad (29)$$

so it is unity for spatially flat models.

If $\Delta^2(k) \propto k^{1.8}$ (so that $\Delta^2_\theta(\ell) \propto \ell^{0.8}$), the angular power scales as

$$\Delta^2_\theta \propto \frac{\int y^{3.2} \phi^2(y) C(y)\,{\rm d}y}{[\int y^2 \phi(y) C(y)\,{\rm d}y]^2} \quad (30)$$

The redshift distribution relates to the selection function via $n(z)\,{\rm d}z \propto y^2 \phi(y) C(y)\,{\rm d}y$. What this says is that the amplitude of angular clustering depends on the range of redshifts that contribute to the sample under study, and a low value of θ_0 requires a large range of redshifts to be contributing.

To be quantitative, consider the results of Giavalisco et al.

(1998) for the angular clustering of Lyman-break galaxies. They deduce $\theta_0 = 2$ arcsec over a redshift range $2.5 \lesssim z \lesssim 3.5$. The relation of comoving distance to observables is

$$C(y)\,\mathrm{d}y = \frac{c}{H_0}\mathrm{d}z \times [(1-\Omega_m-\Omega_v)(1+z)^2+\Omega_v + \Omega_m(1+z)^3]^{-1/2}, \quad (31)$$

and this allows us to see what would happen to the angular clustering signal if the redshift range is extended. Assuming a uniform contribution to the submillimetre surface brightness from $2 < z < 6$, as indicated by the results in earlier sections, the angular clustering signal would be expected to drop by a factor of 0.35 ($\Omega_m = 1$, $\Omega_v = 0$) or 0.34 ($\Omega_m = 0.3$, $\Omega_v = 0.7$) compared to that measured by Giavalisco et al., for the same degree of spatial clustering.

In making this comparison, it is important to be clear that we are including the angular clustering of the ULIRG population, rather than just that of Lyman-break galaxies, since the former give a significant contribution to the background. Nevertheless, the Lyman-break galaxies serve as a useful reference. They are a highly biased population, as indeed would be expected for all reasonably massive galaxies at high redshift (Steidel et al. 1998; Peacock et al. 1998). It would therefore not be surprising if the ULIRG population displayed a similar level of spatial clustering. However, even if this is so, the submillimetre background arises over a broad range of redshifts, and the sky at 850-μm is therefore expected to be more uniform than the Lyman-break sky. Strong clustering of the 850-μm background would only arise if the ULIRGs were much more strongly clustered that Lyman-break galaxies; our results indicate that this cannot be the case.

As a final point, we can now address the question of whether clustering in the background could bias the statistical detection of flux from the UV starburst galaxies. Any given galaxy will statistically be surrounded by a 'halo' of emission contributed by correlated galaxies, whose surface brightness at angular separation θ will be $w(\theta)I$, where I is the mean background. Since we are dealing with two populations, UV starbursts and ULIRGs, in principle we need both the UV–ULIRG cross-correlation function as well as the UV autocorrelation function. However, since a correlation coefficient must be less than unity, the cross-correlation cannot exceed the larger of the two autocorrelations. We can therefore get a limit to the effect by assuming $\theta_0 = 2$ arcsec. The effective point-source flux is obtained by integrating $w(\theta)I_\nu$ over the beam. The result of this exercise is an effective point-source flux density of 0.19 mJy. This is large enough to be a dominant bias for the starbursts with SFR around $1\,h^{-2}\,\mathrm{M}_\odot\,\mathrm{yr}^{-1}$, but cannot erase the signal from the more luminous objects. In order to obtain an upper limit to the overall bias that could be introduced by this effect, the analysis of Section 3.3 for the mean level of 850-μm emission was repeated, subtracting 0.19 mJy from all the flux densities. The result is to reduce the mean submillimetre output for a given SFR by a factor of approximately 2, although we have argued that this is very much an upper limit to the correction. The effect of clustering can therefore in principle have a significant quantitative impact on issues such as the total submillimetre emission from UV starbursts (Section 3.4). However, this does not alter the main point, which is that UV starbursts are one of the largest contributors to the background radiation at these frequencies.

5 CONCLUSIONS

In this paper, we have investigated whether the SCUBA 850-μm map of the HDF can set useful constraints on the general population of optically-selected starburst galaxies, or whether we are confined to investigating only totally obscured ultraluminous infrared galaxies. Although data of improved resolution and sensitivity will be required in order to study the submillimetre properties of HDF galaxies on an individual basis, we believe that there is good statistical evidence that the galaxies detected in the optical HDF catalogues are emitting in the submillimetre band, with a flux density of about $S_{850} = 0.2$ mJy for an apparent UV star-formation rate of $1\,h^{-2}\,\mathrm{M}_\odot\,\mathrm{yr}^{-1}$. This level of emission is consistent with the idea that the UV emission from these galaxies underestimates the total star-formation rate in most cases, by a mean factor of approximately 6. This means that the Lyman-break population must contribute at least 25 per cent of the background radiation at 850 μm.

We have used a variety of tests, including cross-correlation with UV data and power-spectrum analysis of the 850-μm data, to demonstrate that the submillimetre background receives approximately equal contributions from a very wide range of redshifts, $1 \lesssim z \lesssim 6$. Indeed, some of the strongest individual examples of evidence for an association between high-z galaxies and features in the submillimetre map involve galaxies towards the higher end of this range. Together with the lack of a clear optical counterpart for the brightest HDF source (HDF 850.1; Downes et al. 1999), this suggests that the upper bound of the redshift distribution for 850-μm sources may not yet have been reached.

ACKNOWLEDGMENTS

We thank Len Cowie and especially Steve Eales for useful comments on this work. The James Clerk Maxwell Telescope is operated by the Joint Astronomy Centre on behalf of the Particle Physics & Astronomy Research Council of the United Kingdom, The Netherlands Organisation for Scientific Research, and the National Research Council of Canada.

REFERENCES

Almaini O., Lawrence A., Boyle B. J., 1999, MNRAS, 305, L59
Barger A. J., Cowie L. L., Sanders D. B., 1999, ApJ, 518, L5
Barger A. J., Cowie L. L., Smail I., Ivison R. J., Blain A. W., Kneib J.-P., 1999, AJ, 117, 2656
Blain A. W., Kneib J.-P., Ivison R. J., Smail I., 1999, ApJ, 512, L87
Busswell G. S., Shanks T., 2000, astro-ph/0002081
Chapman S. C., et al., 1999, astro-ph/9909092
Downes D., et al., 1999, A&A, 347, 809
Eales S., Lilly S., Gear W., Dunne L., Bond J. R., Hammer F., Le Févre O., Crampton D., 1999, ApJ, 515, 518
Feldman H. A., Kaiser N., Peacock J. A., 1994, ApJ, 426, 23
Fernandez-Soto A., Lanzetta K. M., Yahil A., 1999, ApJ, 513, 34
Fixsen D. J., Dwek E., Mather J. C., Bennett C. L., Shafer R. A., 1998, ApJ, 508, 123
Giavalisco M., Steidel C. C., Adelberger K. L., Dickinson M. E., Pettini M., Kellogg M., 1998, ApJ, 503, 543
Gunn K. F., Shanks T., 1999, astro-ph/9909089
Hauser M. G., et al., 1998, ApJ, 508, 25
Holland W. S., et al., 1999, MNRAS, 303, 659
Hogg D. W., et al., 1998, AJ, 115, 1418
Hughes D., Dunlop J. S., 1999, in Carilli C. L., Radford S. J. E., Menten K. M., Langston G. I., eds, ASP Conf. Ser., Vol. 156, Highly Redshifted

Radio Lines. Astron. Soc. Pac., San Francisco, p. 99 (astro-ph/9802260)
Hughes D. et al., 1998, Nat, 394, 241
Ivison R. J., Smail I., Barger A. J., Kneib J.-P., Blain A. W., Owen F. N., Kerr T., Cowie L. L., 1999, astro-ph/9911069
Jimenez R., Padoan P., Dunlop J., Bowen D., Juvela M., Matteucci F., 2000, ApJ, 532, 152
Kaiser N., 1992, ApJ, 388, 272
Lilly S. J., Le Fèvre O., Hammer F., Crampton D., 1996, ApJ, 460, L1
Lilly S. J., Eales S. A., Gear W. K. P., Hammer F., Le Fèvre O., Crampton D., Bond J. R., Dunne L., 1999, ApJ, 518, 641
Madau P. et al., 1996, MNRAS, 283, 1388
Meurer G. R., Heckman T. M., Lehnert M., Leitherer C., Lowenthal J., 1997, AJ, 114, 54
Meurer G. R., Heckman T. M., Calzetti D., 1999, ApJ, 521, 64
Peacock J. A., 1999, Cosmological Physics. Cambridge Univ. Press, Cambridge
Peacock J. A., Nicholson D., 1991, MNRAS, 253, 307
Peacock J. A., Jimenez R., Dunlop J. S., Waddington I., Spinrad H., Stern D., Dey A., Windhorst R. A., 1998, MNRAS, 296, 1089
Pettini M., Kellogg M., Steidel C. C., Dickinson M., Adelberger K. L., Giavalisco M., 1998, ApJ, 508, 539
Puget J.-L., Abergel A., Bernard J.-P., Boulanger F., Burton W. B., Desert F.-X., Hartmann D., 1996, A&A, 308, L5
Schlegel D. J., Finkbeiner D. P., Davis M., 1998, ApJ, 500, 525
Smail I., Ivison R. J., Blain A. W., 1997, ApJ, 490, L5
Smail I., Ivison R. J., Kneib J.-P., Cowie L. L., Blain A. W., Barger A. J., Owen F. N., Morrison G. E., 1999, MNRAS, 308, 1061
Smail I., Ivison R. J., Owen F. N., Blain A. W., Kneib J.-P., 2000, ApJ, 528, 612
Soifer B. T., Sanders D. B., Madore B. F., Neugebauer G., Danielson G. E., Elias J. H., Lonsdale C. J., Rice W. L., 1987, ApJ, 320, 238
Steidel C. C., Giavalisco M., Pettini M., Dickinson M., Adelberger K. L., 1996, ApJ, 462, L17
Steidel C. C., Adelberger K. L., Dickinson M., Giavalisco M., Pettini M., Kellogg M., 1998, ApJ, 492, 428
Steidel C. C., Adelberger K. L., Giavalisco M., Dickinson M., Pettini M., 1999, ApJ, 519, 1
Thompson R. I., Storrie-Lombardi L. J., Weymann R. J., Rieke M. J., Schneider G., Stobie E., Lytle D., 1999, AJ, 117, 17
Weymann R. J., Stern D., Bunker A., Spinrad H., Chaffee F. H., Thompson R. I., Storrie-Lombardi L. J., 1998, ApJ, 505, L95
Williams R. E. et al., 1996, AJ, 112, 1335

This paper has been typeset from a TEX/LATEX file prepared by the author.